

Figure S1. RSV F-specific B cell sorting, Related to Figure 1.

(A) Gating strategy for a representative infant < 3 mo. (Infant 2026). CD19⁺/CD20⁺ B cells that showed reactivity with RSV F (*right-most plot, quadrant 2*) were single-cell sorted for antibody cloning. B cell reactivity with RSV F probes derived from subtype A and subtype B strains is shown in the top and middle rows, respectively. Index sorting analysis is shown in the bottom row. SSC, side scatter area; FSC, forward scatter area.

(B) Gating strategy for a representative infant \geq 6 mo. (Infant 2042). IgG⁺ or IgA⁺ B cells that showed reactivity with RSV F (*right-most plot, quadrant 2*) were single-cell sorted for antibody cloning. B cell reactivity with RSV F probes derived subtype A and subtype B strains is shown in the top and middle rows, respectively. Index sorting analysis is shown in the bottom row. SSC, side scatter area; FSC, forward scatter area.

(C) Percentage of RSV F-specific, class-switched B cells in each infant. Values shown are derived from flow cytometry data for RSV subtype A.

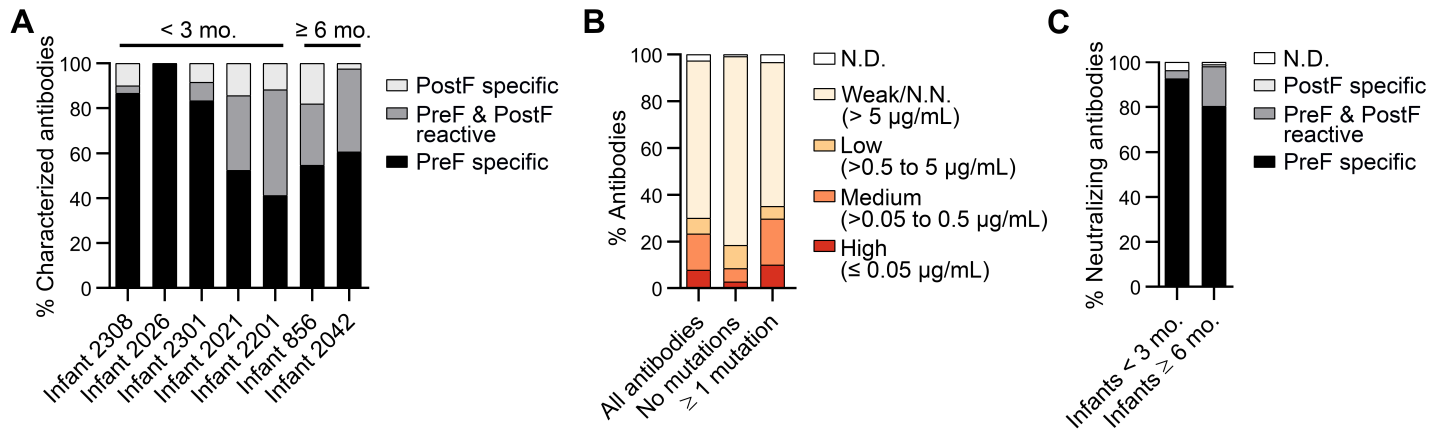


Figure S2. RSV-neutralizing activity increases with SHM and is driven by preF-specific antibodies in young infants, Related to Figure 2.

(A) Percentage of antibodies that were characterized and determined to be preF-specific, preF- and postF-reactive, or postF-specific. Infants are ordered from youngest to oldest, left to right.

(B) Percentage of antibodies with indicated neutralization potencies, grouped according to the number of V-gene nucleotide substitutions.

(C) Percentage of antibodies with indicated preF or postF specificity from infants < 3 mo. and infants ≥ 6 mo.

N.D., not-determined. Results are representative of two independent experiments.

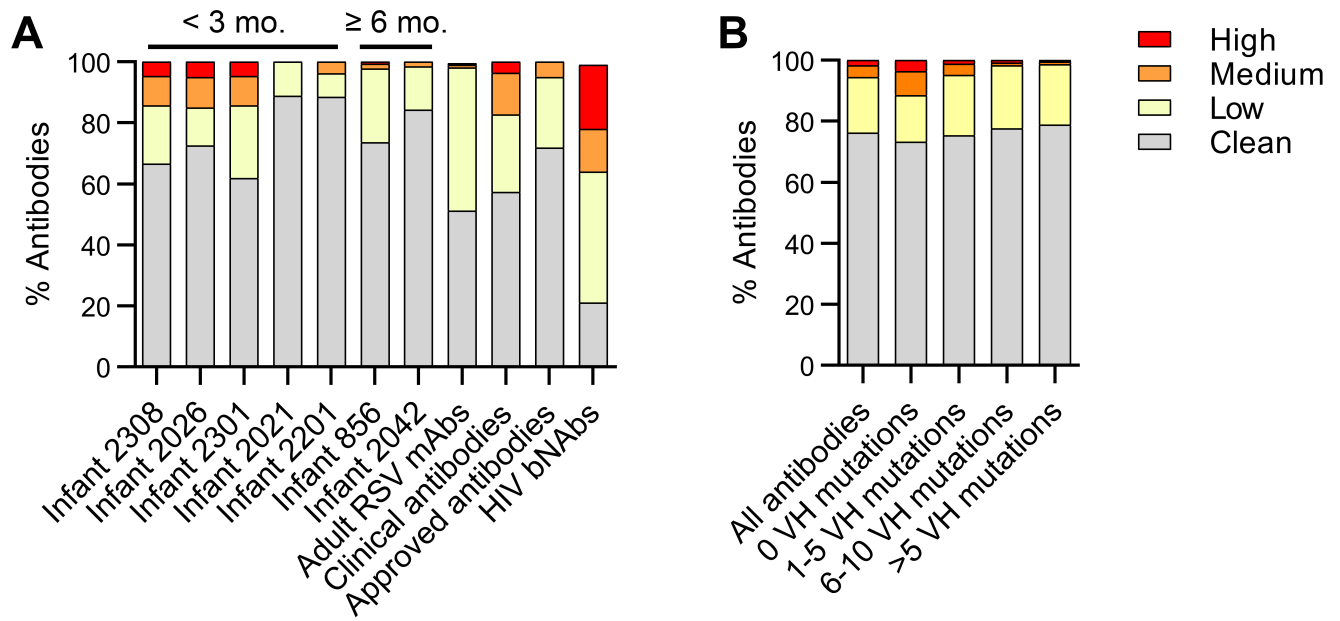


Figure S3. Polyreactivity of infant antibodies decreases with increasing levels of somatic hypermutation, Related to Figure 2.

(A) Percentage of antibodies with high, medium, low, or undetectable polyreactivity (clean), isolated from each infant. Four panels of control antibodies, each with a variety of specificities, are shown for comparison: 364 RSV F-specific antibodies previously isolated from healthy adult donors, 138 antibodies currently in clinical trials, 39 antibodies that are approved for clinical use, and 14 broadly neutralizing HIV-1 antibodies. Colored as in (B). Results are representative of two independent experiments.

(B) Percentage of infant antibodies with high, medium, low, or undetectable polyreactivity (clean), grouped according to the number of VH nucleotide substitutions.

Figure S4. Antibodies directed toward sites I and III show convergent sequence features and preferentially bind to different conformations of RSV F, Related to Figure 3.

(A) Heat map of V-gene usage for site I-directed antibodies. Genes for which no VH:VL pairing was utilized in $\geq 0.5\%$ of site I-directed antibodies are omitted for clarity.

(B) WebLogos of CDR H3 sequences for site I-directed (*top*) and site III-directed (*bottom*) antibodies.

(C) Heat map of V-gene usage for site III-directed antibodies. Genes for which no VH:VL pairing was utilized in $\geq 0.5\%$ of site III-directed antibodies are omitted for clarity.

(D) Apparent (IgG) affinities for postF plotted against affinities for preF for antibodies directed against site I (blue) and site III (green). PreF-specific antibodies are boxed. Affinities of preF-specific antibodies directed against site I and site III (*right*). Results are representative of two independent experiments.

(E) Neutralization potency (IC_{50}) of each antibody, grouped according to antigenic site (*left*). The percentage of antibodies against each site with indicated neutralization potency (*right*). Neutralization IC_{50} values for motavizumab, MPE8, and D25, are indicated by red, purple, and blue dotted lines, respectively. Results are derived from a single experiment performed in duplicate.

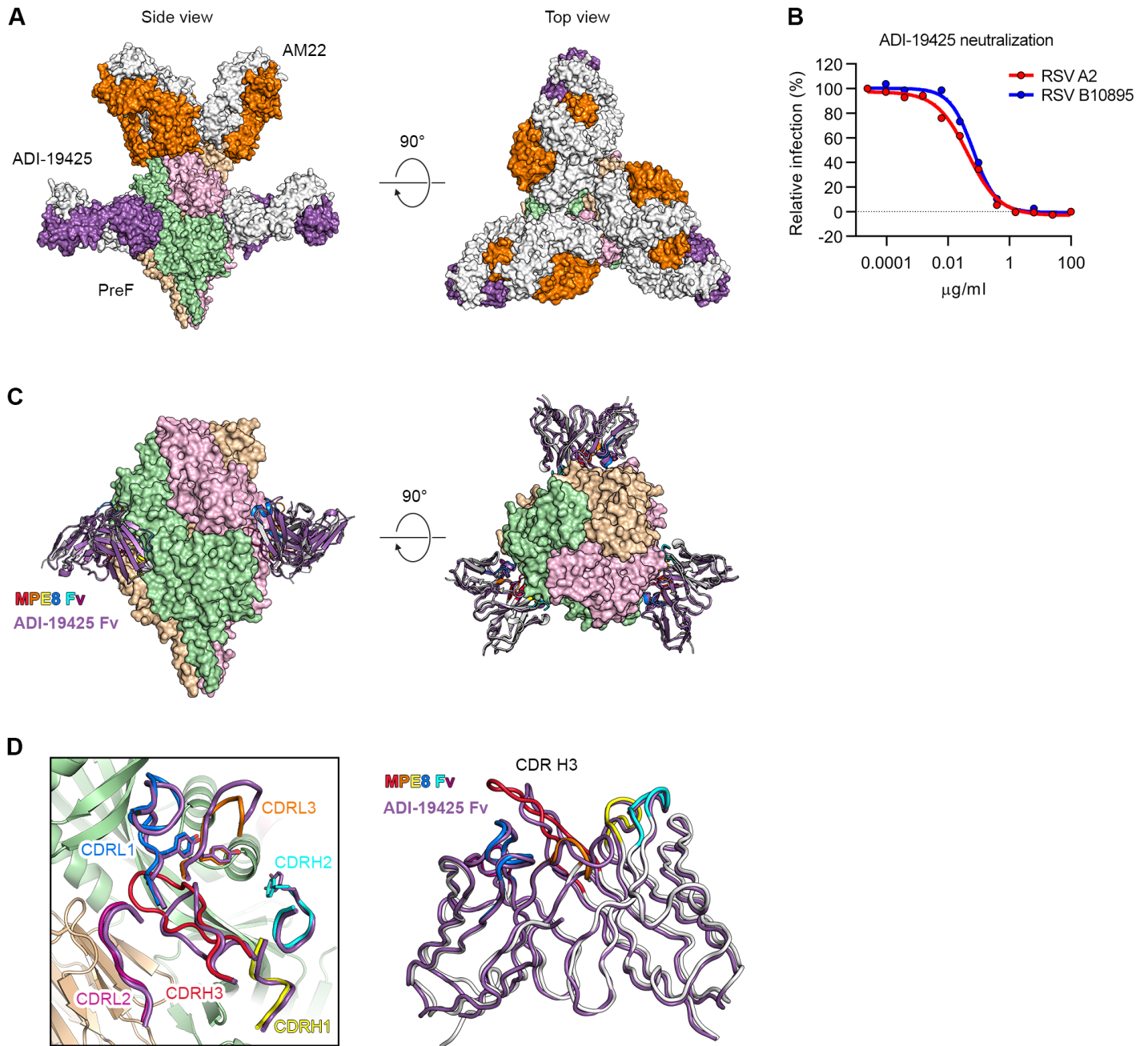


Figure S5. ADI-19425 and MPE8 utilize similar germline-encoded features to recognize preF, Related to Figure 5.

(A) Crystallized ternary complex of preF, AM22 and ADI-19425 is shown as molecular surfaces. The three protomers of preF are shown in pink, green and tan; AM22 heavy and light chains are orange and white, respectively; ADI-19425 heavy and light chains are purple and white, respectively. The same complex rotated by 90° about the horizontal axis to show the view looking toward the viral membrane (*right*).

(B) Neutralization of two RSV strains (A2 and B10895) by ADI-19425 IgG.

(C) PreF from the preF–MPE8 Fv complex (PDB ID: 5U68) aligned to preF from the preF–ADI-19425 complex is shown as molecular surfaces, colored as in (A). ADI-19425 Fv and MPE8 Fv are shown as ribbons and colored purple and white, respectively, with each CDR loop of MPE8 uniquely colored. A 90° rotation of the alignment shows the top view (*right*).

(D) Magnified view of the antibody interface shared by ADI-19425 and MPE8 in the same orientation as Figure 6B (*left*). The variable domains for both ADI-19425 and MPE8 are shown as tubes and colored as in (C). The aligned ADI-19425 and MPE8 variable domains are shown as tubes and colored as in (C) (*right*).

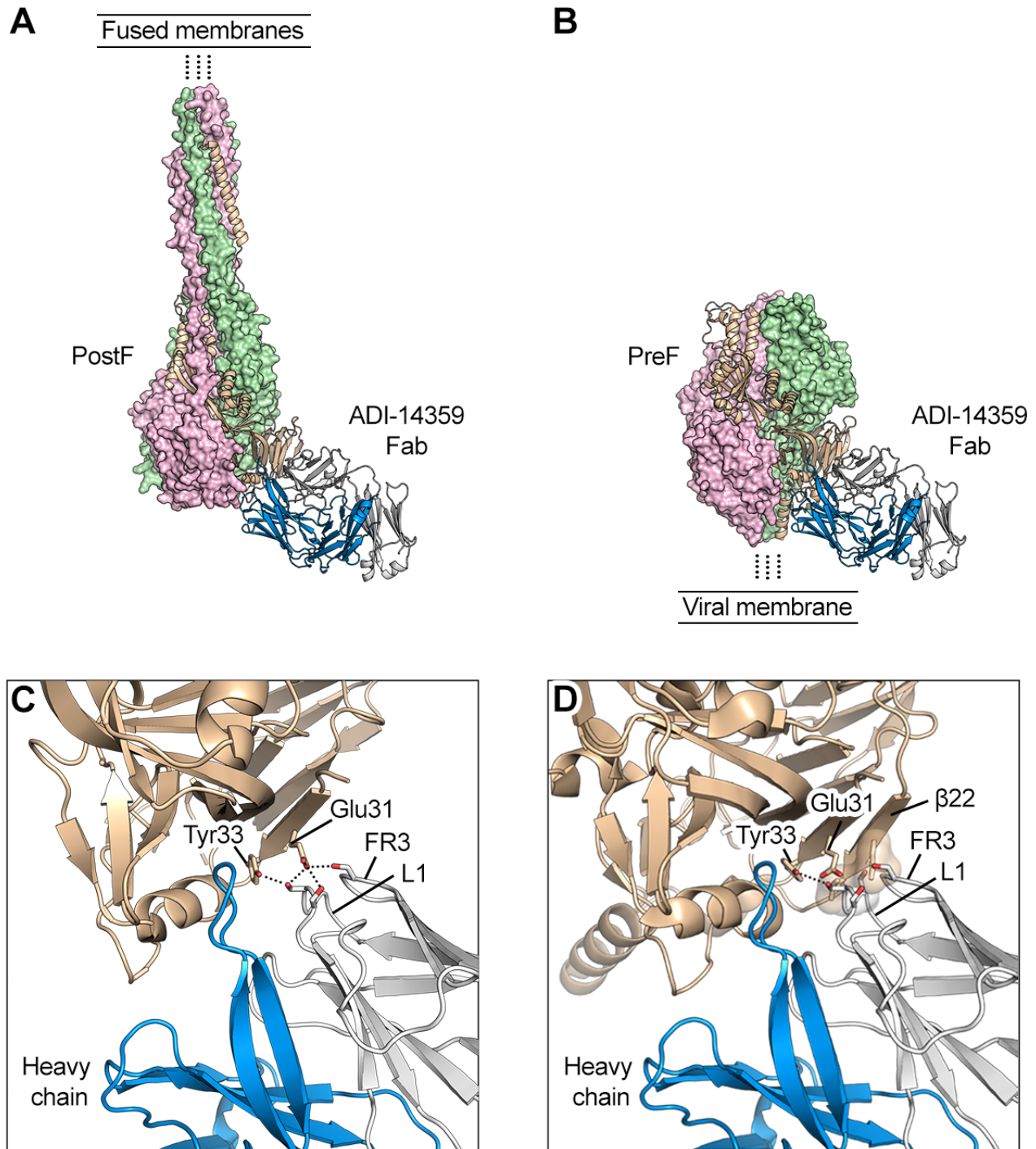


Figure S6. ADI-14359 light chain mediates postF preference, Related to Figure 6.

(A) Crystal structure of ADI-14359 Fab (IGHV2-70:IGKV1-39) in complex with postF. Two protomers of postF are shown as molecular surfaces, and the third protomer and ADI-14359 are shown as ribbons. The ADI-14359 heavy chain is blue and the light chain is white. The position of the fused viral and host-cell membranes is shown for orientation.

(B) Predicted interaction between preF and ADI-14359, determined by aligning the unbound preF structure to the ADI-14359-bound postF structure, colored as in (A). Viral membrane is shown for orientation.

(C) Magnified view of the ADI-14359–postF interface with one protomer shown as tan ribbons. Side chains of residues involved in hydrogen bonding between $\beta 1$ of postF and FR3 or L1 of ADI-14359 are shown as sticks with oxygen atoms colored red. Hydrogen bonds are depicted as black dotted lines.

(D) Magnified view of the predicted ADI-14359–preF interface. Transparent molecular surfaces are shown for residues expected to clash between $\beta 22$ of preF and the FR3 or L1 of the ADI-14359 light chain.

Table S1. Clinical information for infant donors, Related to Figure 1. Blood was drawn from seven infants hospitalized with bronchiolitis and confirmed RSV infection.

ID	Estimated gestational age (weeks)	Birth weight (kg)	Hospital stay (days)	Intensity of care ^a	Intubation	Age at admission (months)	Age at blood draw (months)
2308	39	3.29	5	R	N	0.4	1.4
2026	37	2.41	7	I	N	1.0	2.8
2301	40	4.5	4	R	CPAP	1.5	3.0
2021	33	2.21	15	I	N	1.6	4.5
2201	39	4.39	3	I	N	2.5	12.4
856	32.5	2.07	3	I	N	6.0	10.6
2042	38	3.29	1	I	Y	26.6	29.6

^a R, routine; I, intensive; all patients were administered O₂.

Table S2. Summary of antibody characteristics, Related to Figures 1–4. The name, donor ID number, sequence information, binding affinity, neutralization IC₅₀, epitope and index sort information are shown for each antibody.

Provided as an Excel file for download.

Table S3. Naïve B cells that utilize the IGHV3-21:IGLV1-40 and IGHV3-11:IGHVL1-40 gene pairs recognize site III, Related to Figure 4. Naïve B cell-derived antibodies isolated from cord blood and adult PBMCs were tested for competition with three control Fabs and displayed profiles consistent with recognition of antigenic site III. Results are expressed as fold reduction in antigen binding in the presence of saturating concentrations of competitor Fab relative to an antigen-only control. N.D.; not determined due to low binding affinity.

		Competitor Fab		
		D25	MPE8	Motavizumab
Control IgGs	D25	153	1	1
	MPE8	1	228	20
	Motavizumab	1	1	39
Naïve B cell-derived IgGs	ADI-32365	8	11	19
	ADI-28517	11	23	55
	ADI-32361	7	50	169
	ADI-32367	7	13	35
	ADI-31917	3	69	190
	ADI-31918	2	11	30
	ADI-31919	1	55	159
	ADI-28537	3	52	156
	ADI-31921	3	37	112
	ADI-32360	2	128	416
	ADI-32362	3	117	370
	ADI-32363	2	176	537
	ADI-32366	3	61	210
	ADI-28522	N.D.	N.D.	N.D.
	ADI-31920	N.D.	N.D.	N.D.
	ADI-28523	N.D.	N.D.	N.D.
ADI-28526	N.D.	N.D.	N.D.	
ADI-28527	N.D.	N.D.	N.D.	

Table S4. Crystallographic data collection and refinement statistics, Related to Figures 5 and 6.

	Postfusion RSV F + ADI-14359 Fab	ADI-19425 Fab	Prefusion RSV F + ADI-19425 Fab + AM22 Fab
PDB ID	6APB	6APC	6APD
Data collection			
Space group	<i>P</i> 2 ₁ 2 ₁ 2 ₁	<i>P</i> 2 ₁ 2 ₁ 2 ₁	<i>P</i> 4 ₁ 2 ₁ 2
Cell constants			
<i>a</i> , <i>b</i> , <i>c</i> (Å)	88.5, 99.0, 323.3	61.2, 66.5, 126.0	229.5, 229.5, 304.1
α , β , γ (°)	90	90	90
Wavelength (Å)	1.1809	0.9792	0.9793
Resolution (Å)	51.1-3.0 (3.08-3.00)	26.1-1.7 (1.73-1.70)	50.9-4.1 (4.20-4.10)
Unique reflections	57,978 (4,439)	57,347 (2,940)	64,175 (4,439)
<i>R</i> _{merge}	0.449 (1.662)	0.069 (0.328)	0.364 (1.545)
<i>R</i> _{pim}	0.177 (0.650)	0.028 (0.153)	0.108 (0.443)
<i>I</i> / σ <i>I</i>	5.2 (1.6)	16.8 (4.2)	6.3 (1.9)
CC _{1/2}	0.952 (0.564)	0.998 (0.930)	0.995 (0.609)
Completeness (%)	100.0 (100.0)	99.9 (99.4)	99.9 (100.0)
Redundancy	7.3 (7.4)	6.8 (5.5)	12.2 (13.0)
Wilson <i>B</i> -factors (Å ²)	29	11	118
Refinement			
Resolution (Å)	51.1-3.0 (3.05-3.00)	26.1-1.7 (1.73-1.70)	50.9-4.1 (4.16-4.10)
Unique reflections	57,821 (2,724)	57,181 (2,645)	64,084 (2,497)
<i>R</i> _{work} / <i>R</i> _{free} (%)	22.2/25.5	17.4/20.4	20.4/25.6
No. atoms			
Protein	13,264	3,233	30,005
Ligand/ion	42	10	-
Water	-	692	-
<i>B</i> -factors (Å ²)			
Protein	38	16	166
NAG	63	-	-
SO ₄	-	21	-
Water	-	30	-
R.m.s. deviations			
Bond lengths (Å)	0.004	0.003	0.003
Bond angles (°)	0.86	0.67	0.66
Ramachandran			
Favored (%)	95.9	97.5	95.1
Allowed (%)	3.7	2.1	4.7
Outliers (%)	0.4	0.5	0.2

Values in parentheses are for the highest-resolution shell.

$$R_{merge} = \sum_{hkl} \sum_i |I_{hkli} - \langle I_{hkl} \rangle| / \sum_{hkl} \sum_i \langle I_{hkl} \rangle$$

$$R_{pim} = \sum_{hkl} \sum_i \left(\frac{1}{n_{hkl} - 1} \right)^{1/2} |I_{hkli} - \langle I_{hkl} \rangle| / \sum_{hkl} \sum_i \langle I_{hkl} \rangle$$

$$R_{work} = \sum ||F_{obs}| - |F_{calc}|| / \sum |F_{obs}|$$

R_{free} is the same as R_{work} , but calculated on a randomly selected test set of 5% of the data

$CC_{1/2}$ = Pearson correlation coefficient calculated between intensities of randomly selected half datasets